Oxidation of Metals
https://doi.org/10.1007/s11085-018-9882-1

ORIGINAL PAPER

Use of Microanalysis to Better Understand the High-Temperature Corrosion Behavior of Chromium Exposed to Multi-Oxidant Environments

Satia Soltanattar[1] · Pawel Nowakowski[2] · Cecile S. Bonifacio[2] · Paul Fischione[2] · Brian Gleeson[1]

Received: 15 April 2018

Abstract

The corrosion behavior of metals and alloys at high temperatures in complex multi-oxidant environments is of a great interest for achieving extended service performances and improved operation efficiencies. In this basic study, the scaling reactions of pure chromium in several multi-oxidant gas mixtures were assessed. The environments studied are similar to those that exist in low-NO_x burner and coal gasification atmospheres, which are very reducing and favor sulfidation and carburization, together with possible formation of Cr_2O_3. The effect of sulfur on chromia-scale growth kinetics was also considered. Isothermal exposures were done for up to 100 h at 871 °C (1600 °F), and comparison was made to similar exposures to air. Exposed samples were characterized in detail using some combination of X-ray diffraction and electron beam scattering and spectroscopic techniques. It was found that chromia scales formed in mixed gases containing water vapor grew much faster and had a finer grain structure than those formed in dry air. Both inward growth and outward growth of the chromia scale were inferred for the mixed-gas conditions. The effect of a high carbon potential in the gas on the scaling behavior is also discussed.

✉ Satia Soltanattar
satiaattar@gmail.com

[1] Department of Mechanical Engineering and Materials Science, University of Pittsburgh, 636 Benedum Hall, Pittsburgh, PA 15261, USA

[2] E.A. Fischione Instruments, Inc., Export, PA 15632, USA

Published online: 20 November 2018

Graphical Abstract

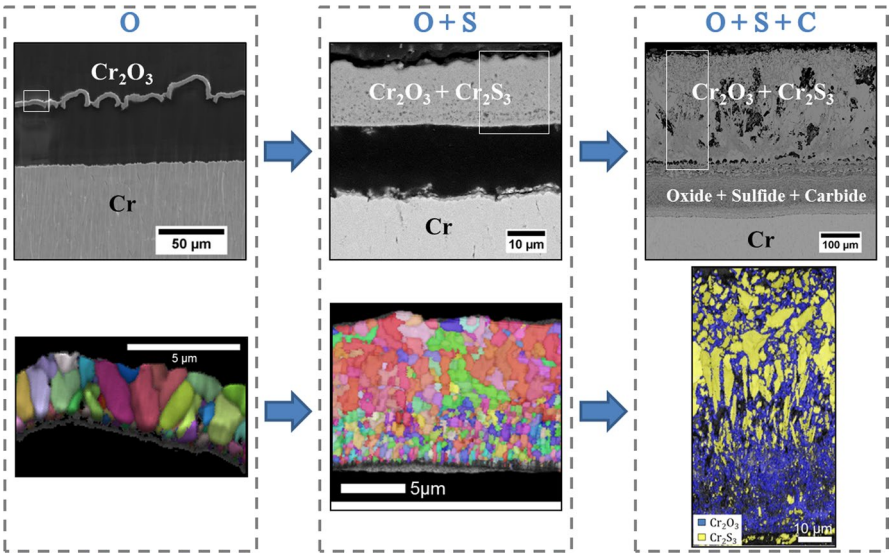

Keywords Mixed gas · Chromia · Sulfidation · Carburization · Water vapor

Introduction

In many process environments such as low-NO_x burners, coal gasifiers or other advanced power systems, alloys are exposed to multi-oxidant gas atmospheres containing low oxygen and high sulfur and carbon activities. Many of these high-temperature alloys rely on formation of a protective slow-growing chromia (or alumina) scale to prevent aggressive attack by oxidants other than oxygen (sulfur, carbon, etc.). However, under some reducing conditions, the alloy may fail to form a protective scale and phases other than oxides may also be stable. In the case of chromia-scale forming alloys, sulfides and carbides of chromium or other alloying elements may form either at the early stages of the reaction or after longer exposure times, which can subsequently cause breakdown of the oxide scale. The presence of these non-oxide phases in the scale can greatly influence the growth kinetics of oxides and associated transport properties by providing short-circuit transport paths and/or a higher defect density. Thus, a considerable increase in the corrosion rate may be observed.

The corrosion mechanism of pure chromium and chromia-forming alloys in different environments of H_2–C_3H_6 [1, 2], CO–CO_2 [2–4], H_2–H_2S [5–7], O_2–SO_2 [2, 8, 9] or other gas mixtures [2, 6, 10–12] has been reported in past studies. Although understanding the mechanisms in environments containing one or two oxidants can be very useful, such environments do not necessarily reflect what occurs under

actual service conditions, which tend to be more complex. Consequently, it is important to identify and analyze corrosion in multi-oxidant environments. The purpose of this study was to investigate the effects of different oxidants in mixed-gas environments on corrosion mechanisms and the morphological development of reaction products on pure Cr in strongly reducing sulfidizing and sulfidizing/carburizing environments at 871 °C (1600 °F). Although chromium is typically used in combination with Ni, Co, Fe and other alloying elements for improved oxidation resistance, a separate study of pure chromium in mixed-gas environments can provide improved understanding of the breakdown mechanism(s) of the thermally grown chromia scales due to the presence of other species in the atmosphere.

Experimental Procedures

Pure chromium of 99.99% purity, procured from Goodfellow Corporation, was used in this study. Test samples were cut to approximate dimensions of $10 \times 10 \times 1$ mm^3. A 1-mm-diameter hole was drilled near the edge of a given sample so that it could be suspended during testing using Kanthal wire. Samples were then polished to 320-grit finish using SiC paper, ultrasonically cleaned and degreased in ethanol and then weighed prior to testing. Samples were then suspended from a sample holder in the furnace. The system was first purged with argon gas for about 20 h to remove oxygen prior to exposing samples to the reaction gas.

Tests were carried out at 871 °C in gas mixtures summarized in Table 1. Water vapor was obtained by flowing the gas through distilled water at a controlled temperature of 0 °C, 23 °C and 46 °C to obtain 0.6, 3 and 10% water vapor, respectively. The pH of the water was stabilized via saturation to ensure achievement of the nominal gas compositions. The equilibrium partial pressures of the gases calculated using HSC software are presented in Table 1 and shown in the Cr–O–S stability diagram in Fig. 1. Cr_2O_3 is seen to be the equilibrium phase in contact with gases 2, 3 and 4. Gas 1, on the other hand, is located very close to the thermodynamic boundary of Cr sulfide/Cr oxide.

With a given gas mixture flowing through the preheated system at a rate of 50 ml/min and linear gas flow rate of 0.05 cm/s, a test was initiated by pushing the samples from a position outside the furnace to inside the hot zone. Sample heating to 871 °C was less than 60 s. A Pt catalyst was positioned at the front (i.e., upstream position) of the hot zone to ensure gas-phase equilibrium. After thermal exposure, samples

Table 1 Equilibrium gas compositions and corresponding equilibrium oxidant potentials at 871 °C (1600 °F) and a total pressure of 1 atm

Gas no.	Gas composition (vol%)	P_{S2} (atm)	P_{O_2} (atm)	a_C
1	N_2–15%CO–3%H_2–0.6%CO_2–0.12%H_2S	1.3×10^{-6}	7.9×10^{-22}	0.2
2	N_2–15%CO–3%H_2–0.6%CO_2–0.12%H_2S + 0.6% H_2O	9.2×10^{-7}	2.1×10^{-20}	0.2
3	H_2–25%CH_4–14.8%N_2–4%CO–0.6%CO_2–0.6%H_2S + 3% H_2O	2.6×10^{-8}	1.3×10^{-22}	~1
4	H_2–25%CH_4–14.8%N_2–4%CO–0.6%CO_2–0.6%H_2S + 10% H_2O	2.2×10^{-8}	4.1×10^{-22}	~1

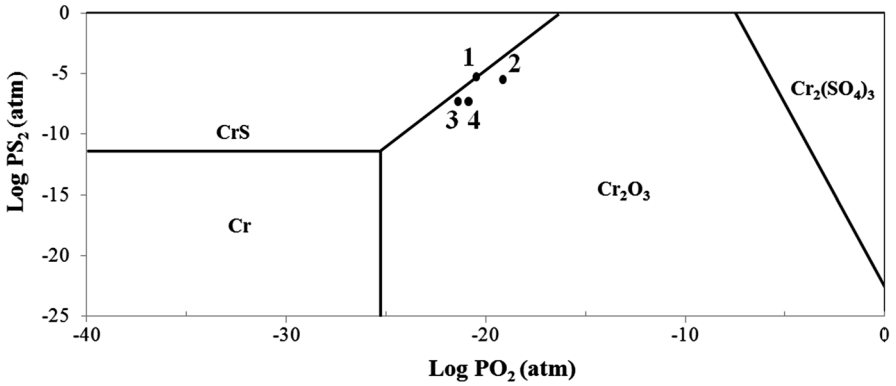

Fig. 1 Phase stability diagram for Cr–O–S system at 871 °C

were removed from the hot zone, cooled to room temperature under argon gas at a normalized rate and then removed from the system for analysis. Additional tests were also carried out in dry-air atmosphere using a Setaram symmetrical thermogravimetric analyzer (TGA) with heating and cooling rates of 99 and 50 °C/min, respectively.

After a given exposure, the specimens were weighed and photographed. Metallographic cross sections were prepared by cold mounting, sectioning and then polishing using standard techniques. Final polishing of the cross-section specimens were performed using a Fischione Instruments Model 1061 by broad-beam Ar ion milling. This method was found to be the best solution for obtaining high-quality cross section without damaging the brittle scale caused by conventional mechanical polishing. Selected specimens were characterized using X-ray diffraction (XRD) prior to mounting. Reaction product morphologies were characterized using scanning electron microscope (SEM), energy-dispersive X-ray analysis (EDX), as well as electron backscatter diffraction (EBSD) and a transmission electron microscope (TEM). The TEM used in this study was a 300 kV FEI TF30 with a field emission gun (FEG), and specimens were prepared using a focused ion beam (FIB) and further thinned using a Fischione Instruments Model 1040 NanoMill® TEM specimen preparation system in order to obtain ultrathin and defect-free foils.

Results

Measured weight changes of pure Cr exposed for 25 h to the four environments at 871 °C are compared in Fig. 2. It is seen that the highest weight gain occurred for the sample exposed to gas 3, which had both high sulfur and carbon activities. The lowest weight gain, however, occurred to the sample exposed to gas 4, which had 10% water vapor. SEM analyses of the corroded cross sections (Fig. 3) showed the formation of a multilayer structure on the sample exposed to gas 1. The scale in this instance consisted of an outer layer of Cr sulfide (56.9S–43.1Cr),

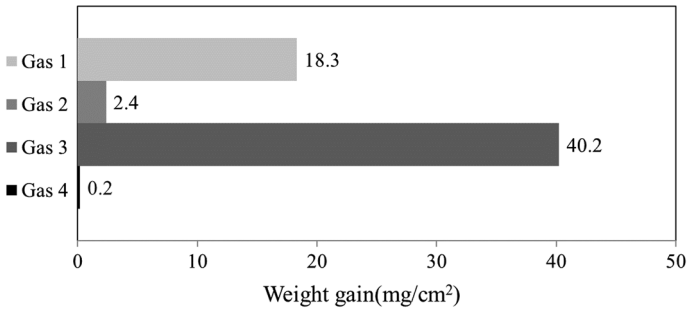

Fig. 2 Weight change measurements after 25 h exposure to the different environments at 871 °C

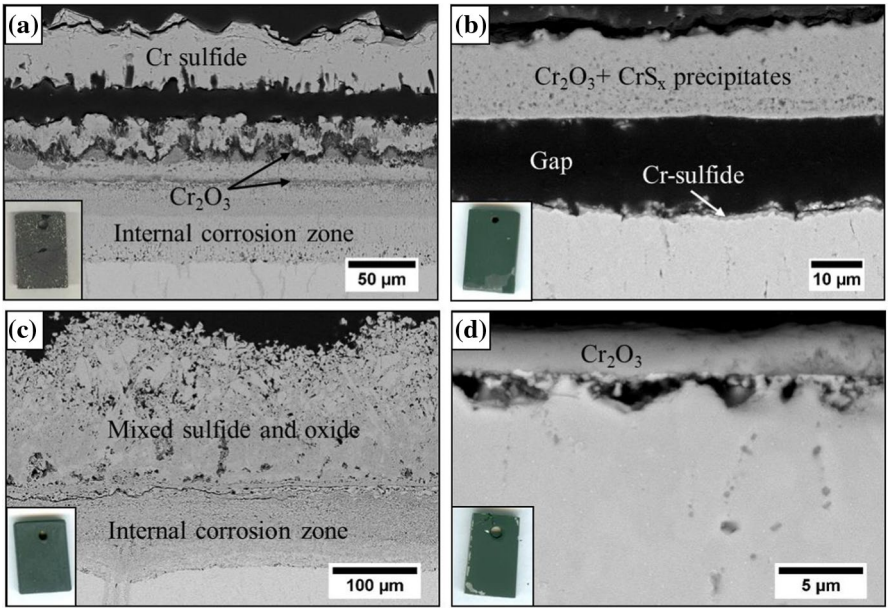

Fig. 3 SEM cross-sectional images of pure Cr after exposure to **a** gas 1, **b** gas 2, **c** gas 3 and **d** gas 4 for 25 h

followed by a thin, intermediate mixed region of Cr oxide and Cr sulfide (38.2O–4.8S–57Cr overall) and a thick inner zone rich in both Cr oxide and Cr sulfide. (All compositions are given in atomic percent, at.%, unless stated otherwise.) In gas 2, a relatively thick and porous Cr_2O_3 layer formed, which contained Cr sulfide particles inside the scale. EDX analysis of the scale showed an average of 7 at.% sulfur in the scale. In gas 3, simultaneous formation of oxide and sulfide occurred, followed by a mixed inner zone. In the case of gas 4 exposure, a continuous chromia scale formed together with void formation at the metal/scale interface. No sulfidation or carburization attack was observed.

Based on the cross-sectional images, it is inferred that gas 3 is very close to the so-called kinetic boundary [5, 13, 14], since simultaneous oxide and sulfide formation had occurred. In addition, exposure to gas 3 resulted in Cr carbide formation in the inner region of the corrosion product. When the chromium sample was exposed to gas 4, it formed solely a Cr_2O_3 scale. This gas had oxygen and sulfur partial pressures lower than those in both gas 1 and gas 2. Moreover, and as will be presented, O_2 is not the main oxidant under these gas conditions. Rather, mass-transfer calculations confirmed that either H_2O or CO_2 is the main reactant.

The effect of atmosphere composition is most interesting in the cases of gases 2 and 3. For the pure chromium exposed to gas 2 for 25 h, the chromia scale that formed was remarkably thick. In addition, by increasing the carbon activity from 0.2 in gas 2–1, in gas 3, more extensive degradation was observed in which the mode of attack changed from oxidation to mixed sulfidation–oxidation–carburization. Thus, key questions to address are the criteria to form a thick chromia scale under conditions of gas 2 and a complex structure resulting from mixed attack under gas 3.

Figure 4 shows an SEM cross-sectional image of pure chromium after exposure to gas 2 for 25 h and the associated EDS maps of oxygen (blue) and sulfur

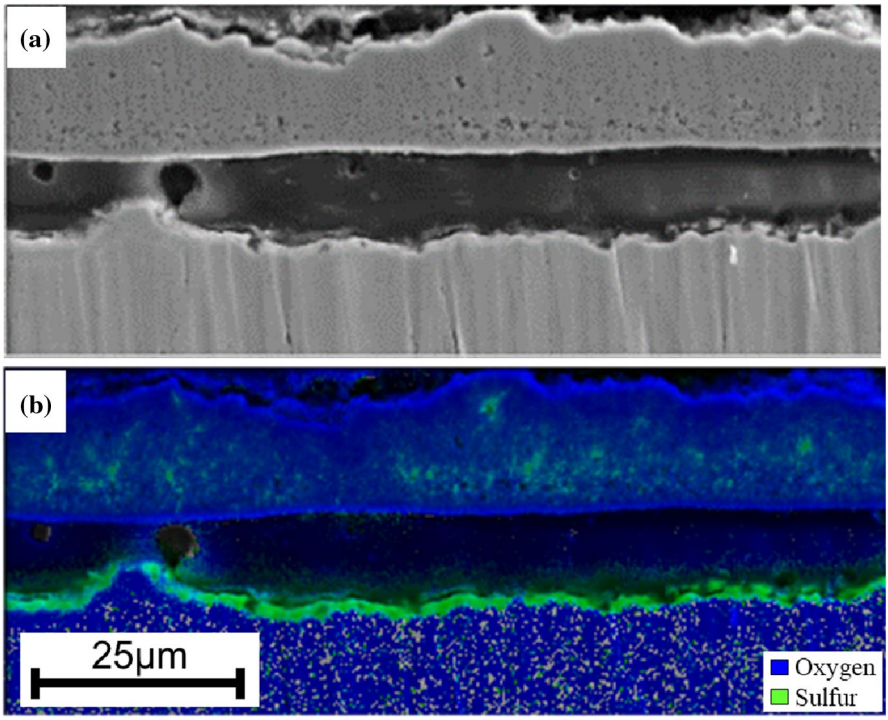

Fig. 4 **a** SEM cross-sectional image of pure Cr after exposure to gas 2 for 25 h at 871 °C and **b** overlapped EDS maps of sulfur and oxygen. The middle region is epoxy resin stemming from detachment of the scale from the metal substrate

(green), which are superimposed. Sulfur is detected throughout the scale. Chromium sulfide precipitates were also present at the metal surface.

Figure 5 presents phase distribution and inverse pole figure (IPF) orientation maps of the scale formed on pure chromium after 25 h exposure to gas 2. The grain structure is mainly equiaxed throughout the scale. However, the grain size varies from the metal/scale interface to the scale/gas interface. According to the orientation map in Fig. 5b, the scale is duplex in structure, with an inner layer comprised of smaller grains with random orientations and an external layer of {0001}-textured larger grains. According to the phase distribution map (Fig. 5a), the scale is primarily chromia. However, small Cr_2S_3 particles with a slightly higher amount along the duplex-layer boundary were observed. This boundary is believed to be the location of the original alloy surface, with the sulfide precipitates formed during the initial stages of exposure and then later overgrown by chromia.

To obtain further insight on the growth mechanism of the scale formed in gas 2, additional experiments with varying exposure times were carried out in this environment. Figure 6 shows the mass change after 5, 10, and 25 h exposure at 871 °C. It is shown that the scaling kinetics increased rapidly between 5 and 10 h exposure. SEM images of the polished cross sections of these samples are presented in Fig. 7. A continuous chromia scale formed after 5 h exposure, together with voids at the metal/scale interface. No sulfide could be detected in the scale or at the metal/scale interface at this stage. The amounts of the initially formed sulfides may be too low to be detected by EDS. The formation of interfacial voids typically is a manifestation of the Kirkendall effect [15] owing to the oxidation of Cr and its outward transport through the scale to react at the scale/gas interface. The relatively thick scale observed after 10 h exposure had a similar structure to that formed after 25 h exposure. The presence of a sulfide layer at the metal/

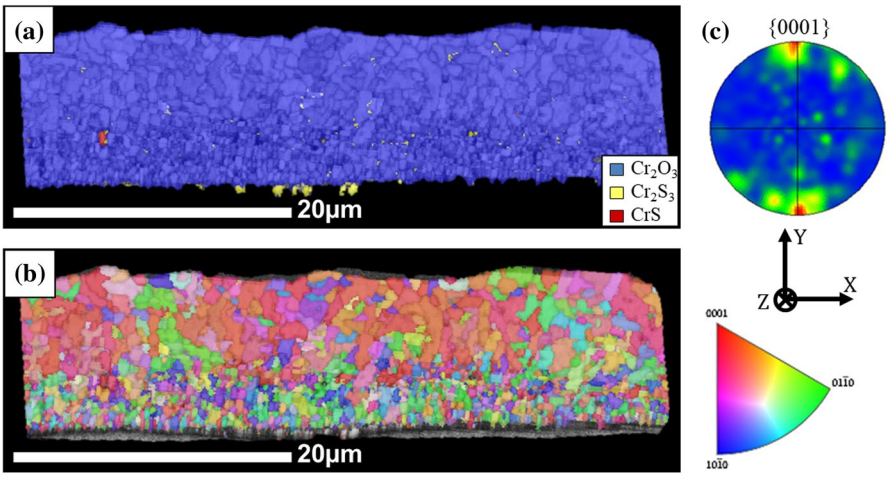

Fig. 5 Electron backscatter diffraction (EBSD) data acquired from the scale formed on pure Cr after exposure to gas 2 for 25 h at 871 °C: **a** phase distribution map, **b** IPF orientation map and **c** pole figure showing {0001} texture

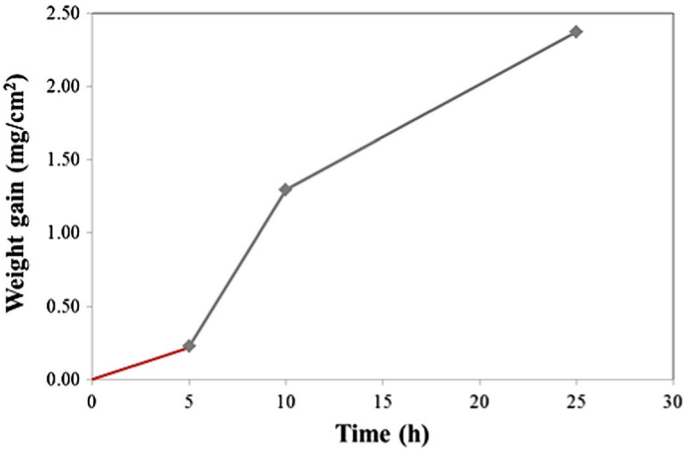

Fig. 6 Measured weight changes for pure chromium exposed to gas 2 at 871 °C for 5, 10 and 25 h

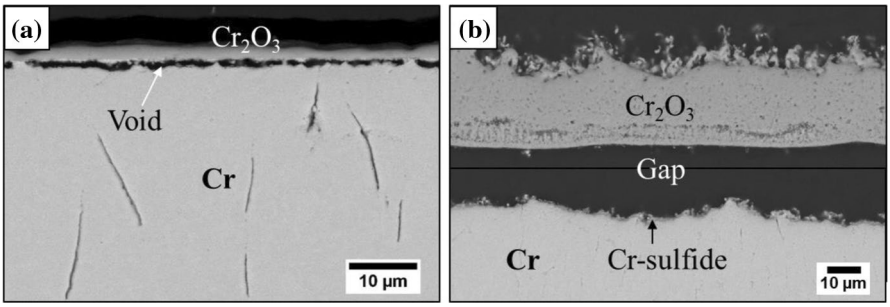

Fig. 7 SEM cross-sectional image of pure Cr after exposure to gas 2 for **a** 5 h and **b** 10 h (the scale after 10 h exposure was detached from the metal substrate; as a result, the position of the scale shown here does not match exactly with the substrate)

scale interface was clearly observed (Fig. 7b). Spallation of the scale can also be observed after 10 h exposure, similar to that after 25 h exposure. Detachment of the scale after 10 h can be attributed, at least in part, to the coalescence of the initially formed voids (observed after 5 h) in addition to imposed thermal and lateral compressive growth stresses, which are known to develop in scales [16–21].

For a more detailed analysis of the sample exposed to gas 2 for 25 h (Fig. 5), two FIB lamellae were prepared for TEM characterization. Figure 8 presents resulting cross-sectional scanning transmission electron microscopy (STEM) images of the scale. The scale has an average grain size of about 440 nm; however, the grain-size distribution varies across the thickness, with larger grains about 640 ± 145 nm (average of 20 grains) in breadth close to the scale/gas interface and smaller grains about 240 ± 70 nm (average of 20 grains) in breadth at the bottom of the scale closer to the metal/scale interface. The void content increases

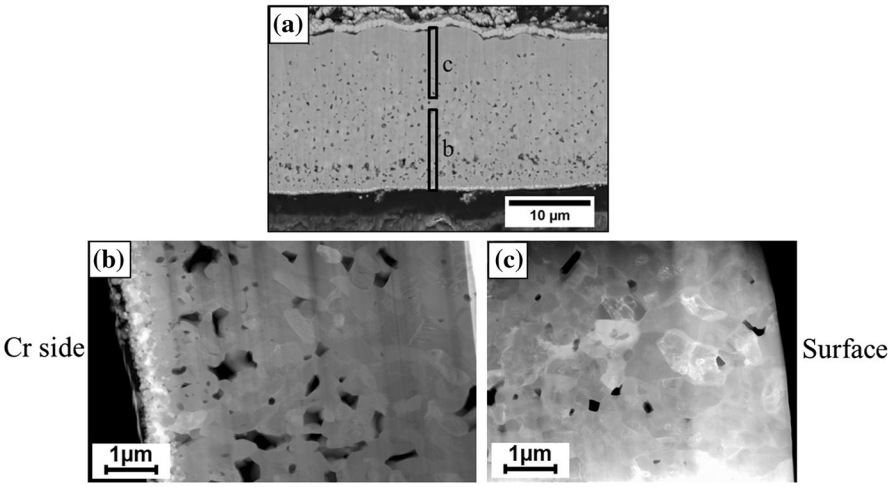

Fig. 8 **a** SEM cross-sectional image of the scale formed on pure Cr after exposure to gas 2 for 25 h at 871 °C with the selected areas for FIB preparation indicated, **b** cross-sectional STEM image of the scale close to Cr/scale interface and **c** cross-sectional STEM image of the scale close to the scale/gas interface

closer to the metal/scale interface, such that the scale close to scale/gas interface is apparently dense.

To better understand the effect of environment on chromia-scale growth, a pure chromium sample was exposed to dry air in a thermogravimetric analysis (TGA) system for 25 h at 871 °C. The weight gain kinetics were found to be in accordance with the parabolic rate law (Fig. 9), with the rate constant, k_p, calculated to be 4.1×10^{-12} g^2 cm^{-4} s^{-1}. This value is in very good agreement with previously reported data [20, 21] which, from interpolation, give a k_p of about 4×10^{-12} g^2 cm^{-4} s^{-1} at 871 °C in oxygen.

As indicated in Fig. 10, the chromia scale that formed after 25 h exposure was detached from the substrate on cooling to room temperature. The scale was also highly convoluted, suggesting the presence of large internal stresses. For reasons that are not clear, the exclusive chromia scale that formed in gas 4 was quite planar, even though it was similar in thickness to the scale formed in air. Presumably the presence of sulfur affected the state of stress in the scale and/or the mode of stress relief. According to the EBSD orientation map, the scale consists of large columnar grains with random orientations and an average grain width of about 940 ± 40 nm (average of 20 grains). Figure 11 shows corresponding cross-sectional STEM images of the scale formed in air. The average scale thickness is around 3.5 μm. The observed columnar grains have an average length of 2.5 μm and width of about 0.9 μm. A much finer grain structure was observed at the bottom of the scale near to the metal/scale interface, which is believed to be the initially formed oxide grains. It is noteworthy that the scale thickness increased from 3.5 μm in air to 17.4 μm in gas 2 for the same exposure time of 25 h.

Significantly greater weight gains were observed for the pure chromium sample exposed to gas 3 compared to other environments. Figure 12a shows a cross-sectional

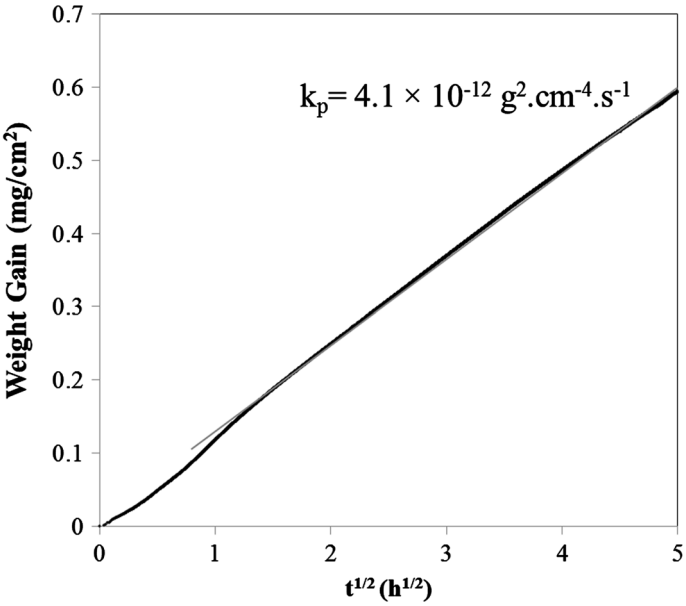

Fig. 9 Measured weight-change kinetics for pure chromium isothermally exposed to untreated air at 871 °C

image of the pure chromium sample exposed to gas 3 for 25 h. The co-formation of chromium oxide and chromium sulfide can clearly be seen from the EDS maps of oxygen and sulfur. The EBSD band contrast and phase distribution maps, Fig. 12b, c, identified the scale constituents to be Cr_2O_3 and Cr_2S_3. The external scale consists of a mixture of sulfide and oxide with an extremely fine grain size at the bottom and larger columnar grains of Cr_2S_3 at the top. The inner attack region (Fig. 13), however, shows three major zones, as indicated by differences in contrast. EDS measurements in each of these zones gave compositions of 51Cr–28S–21O in zone 1, 45Cr–19S–25O–11C in zone 2 and 69Cr–1S–18O–12C in zone 3. The relative differences in carbon content in these zones are more indicative of a trend than anything specific owing to the semi-quantitative nature of the EDS measurement method, particularly for a light element such as carbon. Even so, it is inferred that the carbon content progressively increases from nearly zero in zone 1 to a measurably significant level (~12 at.%) in the innermost zone 3. Sulfur, however, decreases from 28 at.% in zone 1 to about 1 at.% in zone 3, suggesting that the main constituents in the inner corrosion zone are (Fig. 13b): sulfide and oxide in zone 1; sulfide, oxide, and carbide in zone 2; and primarily oxide and carbide in zone 3.

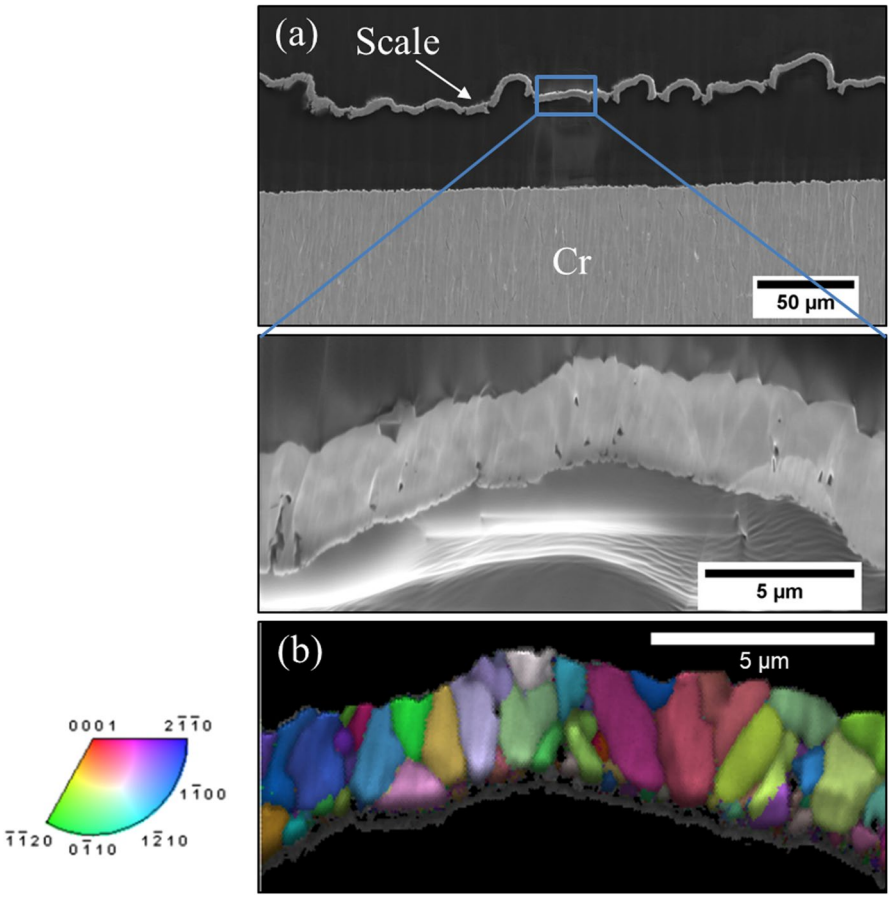

Fig. 10 **a** Cross-sectional SEM image and **b** EBSD inverse pole figure orientation map of pure chromium exposed to dry air for 25 h at 871 °C

Discussion

Gas Flux Calculations

Before proposing any possible corrosion mechanisms under the atmospheres tested, it is informative to ascertain the main oxidant(s). The maximum flux of a given gaseous species *i* to the alloy surface can be approximated by the following expression [22, 23]:

$$J_i = \frac{k_{\mathrm{m}(i)} P_i}{RT} \tag{1}$$

where J is the flux, k_{m} the mass transfer coefficient, P_i the partial pressure of the species i, R the gas constant, and T the temperature. Under laminar flow conditions,

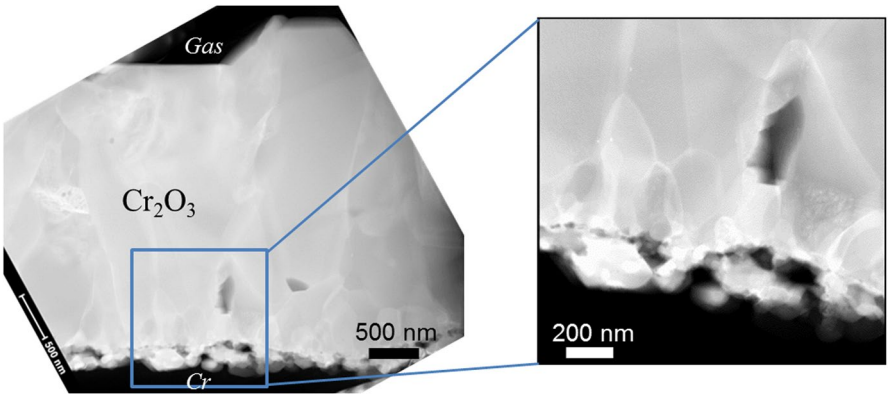

Fig. 11 Cross-sectional STEM image of the scale formed on pure chromium after exposure for 25 h in dry air at 871 °C

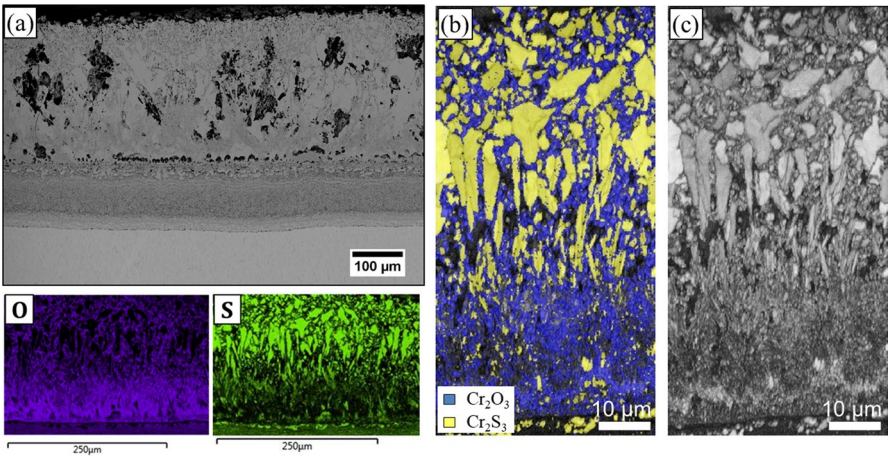

Fig. 12 **a** SEM cross-sectional image and EDS maps of sulfur and oxygen, **b** phase distribution map and **c** EBSD band contrast map of pure Cr after exposure to gas 3 for 25 h

which existed for the current exposures (i.e., Reynolds number calculated to be 0.03), the value of k_m can be estimated from mass-transfer theory via

$$k_m = \mathrm{Sh}\frac{D_{i(N_2)}}{L} \tag{2}$$

Here, L is the sample length, $D_{i(N2)}$ the diffusion coefficient of species i in nitrogen and Sh the Sherwood number. The use of nitrogen gas for calculation of diffusion coefficient of gaseous species i (Eq. 2) is a good approximation for the current discussion. The diffusion coefficient can be calculated from the kinetic theory

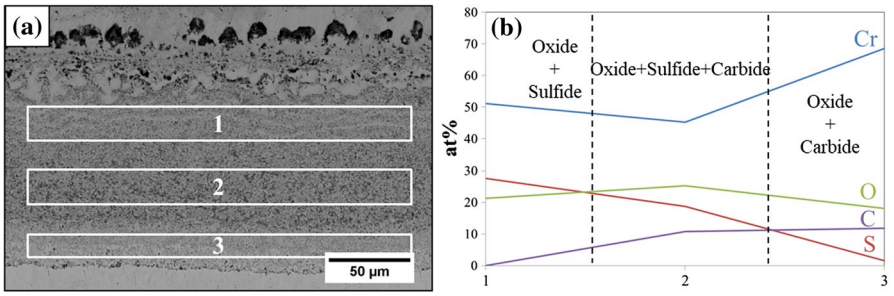

Fig. 13 **a** SEM cross-sectional image and **b** EDS measurements of the inner corrosion zone of pure Cr after exposure to gas 3 for 25 h

of gases as formulated in the Chapman–Enskog equation. The Sherwood number is estimated from the gas density and viscosity. Using calculated k_m values and the equilibrium partial pressures for a given gas mixture, the mass fluxes of O_2, CO_2, H_2O and H_2S were calculated via Eq. (1) and the results are summarized in Table 2.

It should be noted that in an evaluation of mass transfer, the boundary layer thickness is an important parameter. The classical mass transfer theory used in this study assumes boundary layer flow over a flat plate in an unconstrained space. However, for the gas flow in tubular furnace, the boundary layer thickness is significant compared to the tube cross section. This issue was assessed more carefully by Næss et al. [24] in their study of the oxidation kinetics of liquid silicon and using both classical mass transfer calculations and computational fluid dynamics (CFD). The mass transfer rates for SiO (g) obtained from calculation, experiment and CFD modeling were all within the same order of magnitude. This confirmed that under laminar flow conditions, which were also used in the current study, the use of classical mass transfer calculations is valid.

An actual instantaneous oxygen flux for chromia-scale growth can be calculated from the scale thickness formed on Cr after 25 h in gas 4 by assuming

$$x^2 = 2k_P t \tag{3}$$

where x is the scale thickness (cm), t is time (s) and k_P is the parabolic scaling constant in cm^2/s. The oxygen flux necessary to form such a scale is therefore generally given by

Table 2 O_2, CO_2, H_2O and H_2S mass fluxes

	Gas 1		Gas 2		Gas 3		Gas 4	
	P_i (atm)	J_i (g/cm^2 s)	P_i (atm)	J_i (g/cm^2 s)	P_i (atm)	J_i (g/cm^2 s)	P_i (atm)	J_i (g/cm^2 s)
O_2	7.9×10^{-22}	5.6×10^{-26}	2.1×10^{-20}	1.5×10^{-24}	1.3×10^{-22}	9.3×10^{-27}	4.1×10^{-22}	2.9×10^{-26}
CO_2	9.4×10^{-4}	7.8×10^{-8}	4.7×10^{-3}	3.9×10^{-7}	1.6×10^{-4}	1.3×10^{-8}	5.0×10^{-4}	4.1×10^{-8}
H_2O	2.3×10^{-4}	1.0×10^{-8}	1.3×10^{-3}	5.8×10^{-8}	2.5×10^{-3}	1.1×10^{-7}	4.2×10^{-3}	1.9×10^{-7}
H_2S	1.2×10^{-3}	8.2×10^{-8}	1.2×10^{-3}	8.2×10^{-8}	4.6×10^{-3}	3.1×10^{-7}	4.1×10^{-3}	2.8×10^{-7}

$$J_O = \frac{1}{2}\sqrt{\frac{k_P}{t}} \tag{4}$$

which is about 5.1×10^{-10} g/cm^2 s after 25 h of reaction and much higher than the calculated oxygen flux for all four environments (Table 2). Thus, O_2 cannot be the principal oxidant in all gases studied. Knowing that the decomposition of CO_2 is relatively slow [25], H_2O is inferred to be the main oxidant in each environment tested. In accordance with this, the sample exposed to gas 4 had the highest flux of H_2O and formed a continuous and exclusive chromia scale, while the sample exposed to gas 1, which had the lowest H_2O flux, was apparently on the sulfidation side of the Cr sulfide/Cr oxide kinetic boundary, such that sulfidation was the predominant mode of attack.

Microstructural Development in Gas 2

Observations of the chromium samples reacted in different environments illustrate the complex effect of different gas species on the reaction mechanisms. Under conditions of the gas 2 environment with an oxygen partial pressure of about 2.1×10^{-20} atm, a thick duplex chromia scale had formed, followed by sulfide formation at the Cr_2O_3/Cr interface. Chromia-scale growth in H_2O-containing environments with low partial pressures of oxygen has been studied by others [26–29]. Hänsel et al. [29] studied the oxidation of Ni-25Cr at 1000 °C in a low P_{O_2} test gas of Ar–2%H_2–2%H_2O and inferred that oxygen from the water vapor is the principal oxidant for chromia-scale growth. According to these authors, the oxide growth is dictated primarily by the outward diffusion of Cr, which led to Kirkendall void formation at the alloy/scale interface. These voids may subsequently fill with oxide via an H_2–H_2O dissociation process [30, 31]. By contrast, Zurek et al. [26] showed using isotope profiling that Cr_2O_3-scale formation in H_2O-containing environments proceeds by the predominance of inward oxygen grain-boundary diffusion which, in combination with the H_2–H_2O dissociation process, causes better adherence and prevents the establishment of voids at the alloy/scale interface. It is clear from those two recent studies that the growth mechanism of chromia scales in H_2O-containing environments is unresolved.

In the present investigation, a time study was done using pure chromium in gas 2 to more carefully elucidate the growth mechanism. Based on the current results and literature data, the deduced scaling mechanism is summarized schematically in Fig. 14. During the initial stages of the reaction, oxide and sulfide can form simultaneously due to the high H_2O and H_2S fluxes in the gas; however, because Cr_2O_3 is thermodynamically more stable in gas 2 conditions, it can overgrow the initially formed sulfides to establish gas/scale equilibrium. During the scale growth process, voids start to form at the metal/scale interface. The void formation at the Cr/Cr_2O_3 interface clearly resulted from chromium consumption and can, therefore, be interpreted as a sign of outward scale growth during the initial stages of reaction. The interfacial voids were apparently able to persist for a certain period. This is not in agreement with other studies [26, 30–32], which clearly revealed that in water

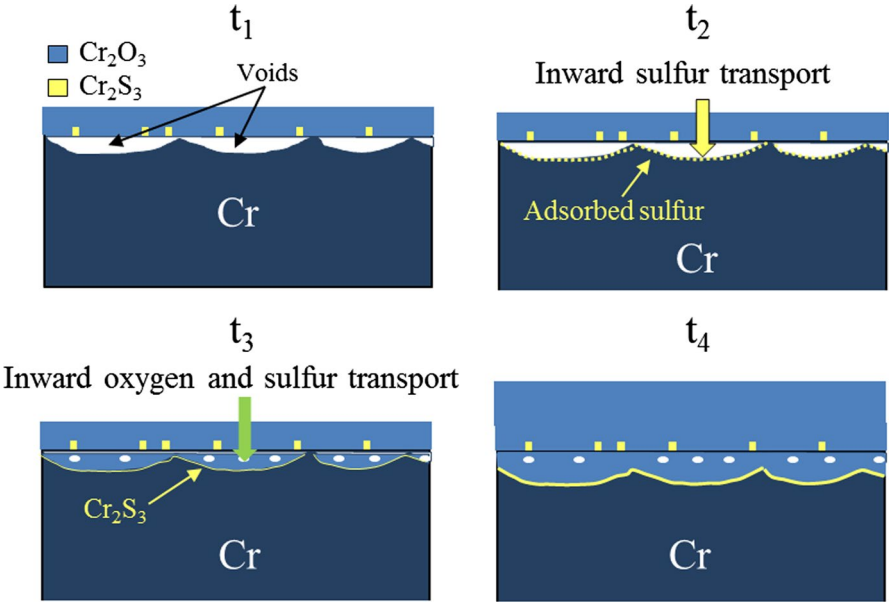

Fig. 14 Schematic of the oxide scaling process on pure Cr in gas 2 at 871 °C with increasing time, t_1 to t_4

vapor-containing environments, the tendency for formation of the interfacial voids and porosity can be eliminated or at least reduced by the rapid gas-phase transport of oxygen within the pore space. A plausible explanation may be linked to the adsorption of sulfur at the internal surfaces of these voids, which poisons the oxidation reaction and, hence, precludes void space filling. Due to the large number of the interfacial voids, scale contact with the substrate is greatly reduced, which restricts Cr supply and consequently causes a relatively low effective growth rate of the scale. However, water vapor can eventually diffuse through the chromia scale and facilitate oxide formation within the void space at the metal/oxide interface. By filling these void spaces, continuity between the scale and substrate metal is achieved and there is a consequent increase in the scaling kinetics (Fig. 6). Such a mechanism can result in the formation of a duplex layer, where the outer scale growth is dictated by cation diffusion and the inner zone is the result of the oxide growth within the metal consumption zone.

In the cases where the chromia scale grows by outward chromium diffusion (especially in the absence of H_2O and at high P_{O_2} levels), formation of a large columnar grain structure is reported [26–29]. Under such conditions, the oxide grains at the free surface can easily grow in size without any constraints. Similar behavior was observed in this study with the sample exposed to the dry-air atmosphere. However, comparison of the results between dry and wet atmospheres suggests that water vapor in the environment interacts with oxide grain boundaries. According to Young [27], under wet oxidizing conditions, the H_2O molecules can be adsorbed on the oxide grain boundaries and hinder their movement and grain growth. What results is a fine-grained equiaxed structure. It was also reported by Galerie et al. [33] that in

the presence of water vapor and at lower P_{O_2} levels, the growth mechanism changes to inward growth, possibly due to the transport of hydroxyl ions along the grain boundaries. By contrast, in the current study, the grain structure observed in the outer scale (believed to grow by outward diffusion of cations) after exposure to gas 2 was more equiaxed and the grain size was much smaller than in dry air. Indeed, adsorption of H_2O molecules may be causing the change in grain size and structure. However, the sulfur- and carbon-containing species in the environments used in this study may also be a factor by adsorbing on grain boundaries and, thus, affecting their movement and growth. Specifically, under such conditions, nucleation is favored over growth and a fine equiaxed grained scale structure results. Competitive adsorption of different species on internal surfaces of the scale, such as grain boundaries, has been reported previously [34–37]. Young and Watson [2] and Zheng and Young [12] also showed that the presence of sulfur and water vapor in the atmosphere affects the transport properties of other species, such as carbon and nitrogen, through the scale. The results observed by other researchers and the results observed in this study together strongly indicate the ability of sulfur-containing species and water vapor in the gas to interact with internal surfaces of a chromia scale, to the extent that transport properties are changed and the scaling mechanism is affected. The grain-boundary diffusion contribution to the scaling kinetics will be discussed next.

Grain Size Effect

Although an exclusive chromia scale had formed under both gas 2 and dry-air conditions, it was observed that scaling was much faster in the former. According to the TEM cross-sectional images of these two specimens, the oxide scale formed in the dry air showed large grains with a columnar morphology. In contrast, the oxide formed in the gas 2 was polycrystalline with a very small grain size. These results suggest that the faster scale growth in gas 2 proceeds to a large extent via relatively rapid grain-boundary diffusion. Considering that the oxide grew according to parabolic kinetics in both gas 2 and dry air, the scale thickness at a given time is given by the rate law in Eq. (3).

According to the Wagner's theory [38], the oxidation kinetics are controlled by the transport properties of the oxide scale. As summarized by Atkinson [39], the following expression for the parabolic rate constant is related to the tracer self-diffusion coefficients D^* in the oxide (Mo_α),

$$k_{\mathrm{P}} = \int_{I}^{II} \left(\alpha \frac{D^*_{\mathrm{M}}}{f_{\mathrm{M}}} + \frac{D^*_{O}}{f_{O}} \right) \mathrm{d}\left(\ln a_{\mathrm{O}_2} \right) \tag{5}$$

where f is the correlation coefficient for diffusion, a_{O2} is the molecular oxygen activity (approximately equal to the partial pressure of oxygen) and the limits of integration are the metal/scale (I) and scale/gas (II) interfaces.

In the case of Cr_2O_3-scale formation, the existing data show that the oxide itself has very good protective properties and the reported lattice diffusion coefficients are extremely low [39]. In fact, the reported diffusion coefficients are far too low to explain the oxidation rates observed for chromium under the different environments used in this study. According to the literature [39–42], grain-boundary diffusion coefficients are orders of magnitude faster than the coefficients for lattice diffusion. The contribution of grain-boundary diffusion can be represented in an effective diffusion coefficient D^*_{eff} given by [43]

$$D^*_{\text{eff}} \simeq D_{\text{Lattice}} + 2\frac{\left(D_g\delta\right)^*}{g} \tag{6}$$

where D_{Lattice} is the lattice and D_g is the grain-boundary diffusion coefficient, δ is the grain-boundary thickness and g is the grain size of the oxide scale. Using Eq. (6), if it is assumed that the grain boundary thickness, δ, is the same in two gases 2 and dry air (there may be some variations for δ in the scales formed in these gases. however, very likely not close to the variations in g) and taking $D_g \gg D_{\text{Lattice}}$, the ratio of effective diffusion coefficients in gas 2 and dry air can be written as

$$\frac{D^*_{\text{eff (gas 2)}}}{D^*_{\text{eff (dry air)}}} = \frac{g_{\text{dry air}}}{g_{\text{gas 2}}} \tag{7}$$

for the oxide scales having grain sizes of 440 nm (gas 2) and 940 nm (dry air); this ratio is calculated to be around 2.1. However, using D^*_{eff} in Eq. (5) gives

$$k_P = \int_I^{II} D^*_{\text{eff}} \mathrm{d}\left(\ln a_{O_2}\right) \tag{8}$$

and knowing the scale thickness, reaction time and partial pressures of oxygen at both interfaces, the ratio of effective diffusion coefficients in gas 2 to dry air is calculated to be 110, which is far higher than the calculated 2.1 based on the grain-size measurements. Thus, grain-boundary diffusion cannot solely account for the observed oxidation rates in gas 2. This shows that the scale formed under the conditions of gas 2 contains even faster transport pathways, perhaps due to the presence of other species (sulfur- or carbon-containing species) in the gas affecting D_g in some way that is currently not understood in chromia-scale systems.

A previous study by Heuer et al. [44] on alumina scales showed that both grain-boundary diffusion coefficients of Al (D_g^{Al}) and oxygen (D_g^{O}) are orders of magnitude larger than lattice diffusion (10^5 for Al and 10^8 for oxygen). Moreover, it was also shown that not all grain boundaries are equal when it comes to enhanced diffusion. The diffusion properties of the scale can vary according to the differences in diffusion coefficients along random high-angle grain boundaries. That study along with others [45, 46] clearly showed that oxygen diffusivities in alumina scales can vary by a factor of 10^3, depending on the grain boundary character and atomic structures.

In this study, the measured grain-boundary diffusion coefficient in the chromia scale formed in gas 2 is higher than that formed in dry-air atmosphere by a factor of 10^2, which is within the 10^3 range reported for diffusivities in alumina scale. Thus, it is possible that the significantly enhanced diffusion in the chromia scale formed in gas 2 could also be due to the higher diffusion coefficient of the grain boundaries aligned in the growth direction of the scale. The predominance of one orientation in the outer scale of the sample exposed to gas 2 compared to that exposed to dry air might also be due to the sulfur presence at the internal surfaces such as grain boundaries, favoring a specific rapid transport orientation. Further investigation of these hypotheses for Cr_2O_3 scales is clearly needed.

Microstructural Development in Gas 3

The scale formed during exposure to gas mixture 3 contained both oxide and sulfide. The total weight gain per unit area was much greater than that for gas mixture 2 (see Fig. 2). Continuous sulfide paths through the entire scale thickness were observed, with larger sulfide grains close to the scale/gas interface. It should be noted that although the calculated equilibrium partial pressure of sulfur (P_{S2}) is lower in gas 3 compared to gas 2, the flux of H_2S to the surface of the sample is more than three times higher, which can increase the relative amounts of sulfide formation at the initial stages compared to oxide. LaBranche and Yurek [5] previously studied the effect of P_{H_2O}/P_{H_2S} ratio on oxidation resistance of pure chromium in carbon-free H_2–H_2O–H_2S gas mixtures at 900 °C. They showed that a critical value of the P_{H_2O}/P_{H_2S} ratio in the environment is necessary to promote formation of a protective Cr_2O_3 scale over the metastable sulfide. Based on their observations, this critical value of the P_{H_2O}/P_{H_2S} ratio for pure chromium at 900 °C was determined to be between 3 and 10. In this study, exposure of chromium to the gas mixture 3 with a $P_{H_2O}/P_{H_2S}=0.5$ resulted in a more aggressive attack than what was observed for gas mixture 2 with $P_{H_2O}/P_{H_2S}=1.1$. Even though Cr_2O_3 is still the thermodynamically more stable phase in gas mixture 3, the observed co-formation of oxide and sulfide in the outer scale indicates that the kinetic boundary of Cr oxide/Cr sulfide in Cr–O–S phase stability diagram is slightly shifted to the right, where gas 3 is now located on this boundary. As a result, the initially formed metastable sulfides can continue to grow due to the kinetic factors, which will result in a fast-growing scale comprised of Cr oxide and Cr sulfide. The fast growth rate of the scale under such conditions is a consequence of both continuous diffusion pathway through the sulfide phase and the phase boundaries of oxide/sulfide, which can act as fast diffusion pathways. It should also be noted that the presence of other species, most importantly carbon, can affect the oxide/sulfide transition and the corrosion mechanism. A comparison of the results observed in this study with those of LaBranche and Yurek [5] suggests that presence of carbon in the environment can affect the required P_{H_2O}/P_{H_2S} for the formation of protective oxide scale, such that this ratio can be lower in the carbon-containing gas. But this is not to state that carbon is beneficial, as this study clearly showed that more aggressive attack occurred in gas 3 which had the high carbon activity and comparatively low P_{H_2O}/P_{H_2S} ratio.

Regarding gas 3, a relatively deep porous inner corrosion zone was observed after 25 h exposure. The average EDS measurements across the inner attack zone confirmed the formation of the Cr carbide at the reaction front (Fig. 13). Formation of the inner corrosion zones depends on the ability of different oxidants in the gas to penetrate the scale. It has been shown [2, 3, 12] that carbon penetrates the Cr_2O_3 scale primarily by molecular transport through internal surfaces and physical imperfections. The mixed interwoven oxide–sulfide structure of the external scale with phase boundaries aligned in the diffusion direction appears to increase the carbon permeability toward the scale/metal interface compared to only oxide grain boundaries in the sample exposed to gas 2. The increased carbon permeability led to an increase in carbon activity at the scale/metal interface, where oxygen activity is lowest. As a result, the carbide was stable to form. Finally, the sulfide also dissociated at the heavily voided metal/scale interface (formed mainly due to the rapid outward growth of the mixed scale) and released sulfur, which could subsequently go on to form Cr sulfides. In accordance with the analysis presented by Meijering [47], the sequence of phases formed occurred in the order of thermodynamic stability, with the most stable phase (oxide) at the surface and the least stable (carbide) at the bottom. Furthermore, the higher carbon activity in gas 3 might play a more important role in changing the reaction pathway as compared to gas 2 by affecting the corrosion mechanism at initial stages of reaction. However, a clearer understanding of the effect of carbon requires further investigation.

Conclusions

High-temperature exposure to mixed sulfidizing–carburizing–oxidizing environments is a complex and dynamic process that requires oxide-scale formation for protection. However, the mode of growth and kinetics of oxide formation are clearly affected in the presence of sulfur and carbon in the atmosphere.

Gas 2 with the P_{H_2O}/P_{H_2S} ratio of 1.1 is located close to the kinetic boundary of Cr oxide/Cr sulfide at 871 °C, but is still within the oxide stable region. The formation of a relatively thick chromia scale was observed after 25 h exposure. Kinetic analysis that considered gas supply and consumption showed that under such conditions, H_2O or CO_2 is the main reactant in the environment. The kinetically easier dissociation of H_2O leads to the inference that it is the principal reactant. The observed chromia scale was shown to form by a combination of both outward growth and inward growth, where the outer scale growth is dictated by cation diffusion and the inner zone is the result of the oxide growth within the metal consumption zone.

It was shown that the fine-grain structure of the chromia scale in the gas 2 environment cannot solely account for fast oxidation kinetics observed in the mixed environments. The adsorbed sulfur affecting the grain boundary structure of the scale and the higher diffusion coefficient of the grain boundaries aligned in the growth direction of the scale are inferred to affect the grain-boundary diffusion.

Void formation due to the initial outward scale growth was observed at the alloy/scale interface. Sulfur adsorption at the scale/metal interfacial voids and sulfur

poisoning at the void surfaces are believed to be the main reasons for an initial period of oxide formation inside the voids being impeded.

Exposure of chromium to the gas mixture 3 with a relatively low P_{H_2O}/P_{H_2S} ratio of 0.5 resulted in a more aggressive attack than what was observed for gas mixture 2 with a P_{H_2O}/P_{H_2S} ratio of 1.1. Formation of a duplex Cr oxide/Cr sulfide outer scale indicates that the kinetic boundary of Cr oxide/Cr sulfide in the Cr–O–S phase stability diagram is slightly shifted to the right, where gas 3 is located on this boundary. Increasing the carbon activity, in addition to the lower P_{H_2O}/P_{H_2S} in gas 3, caused the co-formation of oxide and sulfide in the external scale and deep oxide–carbide–sulfide inner corrosion zones.

Acknowledgements The authors would like to thank Prof. Gerald Meier for helpful discussions and Dr. Sahar Farjami for technical assistance on EBSD sample preparation and microscopy.

References

1. H. J. Grabke, *Corrosion Science* **56**, 2000 (801).
2. D. J. Young and S. Watson, *Oxidation of Metals* **44**, 1995 (239).
3. T. D. Nguyen, J. Q. Zhang and D. J. Young, *Materials at High Temperatures* **32**, 2015 (16).
4. C. S. Giggins and F. S. Pettit, *Oxidation of Metals* **14**, 1980 (363).
5. M. H. LaBranche and G. J. Yurek, *Oxidation of Metals* **28**, 1987 (73).
6. K. Natesan, *Corrosion-NACE* **41**, 1985 (646).
7. A. Rahmel, M. Schorr, A. Velasco-Tellez and A. Pelton, *Oxidation of Metals* **27**, 1987 (199).
8. C. D. Asmundis, F. Gesmundo and C. Bottino, *Oxidation of Metals* **14**, 1980 (351).
9. F. Gesmundo, *Oxidation of Metals* **13**, 1979 (237).
10. M. A. Harper and J. P. Cotner, *Oxidation of Metals* **53**, 2000 (427).
11. J. A. Kneeshaw, The corrosion behavior of Fe–Cr–Ni alloys in complex high temperature gaseous atmospheres containing the reactants oxygen, sulphur and carbon. Doctoral Dissertation, Loughborough University, 1987.
12. X. G. Zheng and D. J. Young, *Materials Science Forum* **251–254**, 1997 (567).
13. R. A. Perkins, in *DOE, EPRI, GRI, NBS, Third Annual Conference on Materials for Coal Conversion and Utilization*, October 10-12, 1978.
14. M. F. Stroosnijder and W. J. Quadakkers, *High Temperature Technology* **4**, 1986 (141).
15. A. D. Smigelskas and E. O. Kirkendall, *Transactions of AIME* **171**, 1947 (130).
16. H. Hindamtw and D. P. Whittle, *Oxidation of Metals* **18**, 1982 (245).
17. D. Caplan, A. Harvey and M. Cohen, *Corrosion Science* **3**, 1963 (161).
18. F. A. Golightly, G. C. Wood and F. H. Stott, *Oxidation of Metals* **14**, 1980 (217).
19. F. A. Golightly, F. H. Stott and G. C. Wood, *Oxidation of Metals* **10**, 1976 (163).
20. K. P. Lillerud and P. Kofstad, *Journal of Electrochemical Society* **127**, 1980 (2397).
21. P. Kofstad and K. P. Lillerud, *Journal of Electrochemical Society* **127**, 1980 (2410).
22. D. R. Gaskell, *An Introduction to Transport Phenomena in Materials Engineering*, (Macmillan, New York, 1992).
23. D. R. Poirier and G. H. Geiger, *Transport Phenomena in Materials Processing*, (The Minerals, Metals & Materials Society, Warrendale, 1994).
24. M. K. Næss, D. J. Young, J. Zhang, J. E. Olsen and G. Tranell, *Oxidation of Metals* **78**, 2012 (363).
25. D. J. Young, *High Temperature Oxidation and Corrosion of Metals*, (Elsevier, Oxford, 2008).
26. J. Zurek, D. J. Young, E. Essuman, M. Hansel, H. J. Penkalla, L. Niewolak and W. J. Quadakkers, *Materials Science and Engineering A* **477**, 2008 (259).
27. D. J. Young, *Materials Science Forum* **595–598**, 2008 (1189).
28. L. Latu-Romain, Y. Parsa, S. Mathieu, M. Vilasi, M. Ollivier, A. Galerie and Y. Wouters, *Oxidation of Metals* **86**, 2016 (497).
29. M. Hänsel, L. Garcia-Fresnillo, S. L. Tobing and V. Shemet, *Materials at High Temperatures* **29**, 2012 (187).

30. A. Rahmel and J. Tobolski, *Corrosion Science* **5**, 1965 (333).
31. C. T. Fujii and R. A. Meussner, *Journal of the Electrochemical Society* **111**, 1964 (1215).
32. M. Michalik, M. Hänsel, J. Zurek, L. Singheiser and W. J. Quadakkers, *Materials at High Temperatures* **22**, 2005 (213).
33. A. Galerie, Y. Wouters and M. Caillet, *Materials Science Forum* **369–372**, 2001 (231).
34. H. J. Grabke, *Materials Science and Engineering* **42**, 1980 (91).
35. R. G. Olsson and E. T. Turkdogan, *Metallurgical Transactions* **5**, 1974 (21).
36. T. A. Ramanarayanan, *Materials Science and Engineering* **87**, 1987 (113).
37. J. Barnes, J. Corish and J. F. Norton, *Oxidation of Metals* **26**, 1986 (333).
38. C. Wagner, *Zeitschrift für Elektrochemie* **63**, 1959 (772).
39. A. Atkinson, *Materials Science and Technology* **4**, 1988 (1046).
40. A. C. S. Sabioni, A. M. Huntz, J. Philibert and B. Lesage, *Journal of Materials Science* **27**, 1992 (4782).
41. R. E. Lobnig, H. P. Schmidt, K. Hennesen and H. J. Grabke, *Oxidation of Metals* **37**, 1992 (81).
42. A. M. Huntz and S. C. Tsai, *Journal of Materials Science Letters* **13**, 1994 (821).
43. A. Atkinson, *Reviews of Modern Physics* **57**, 1985 (437).
44. A. H. Heuer, M. Zahiri Azar, H. Guhl, M. Foulkes, B. Gleeson, T. Nakagawa, Y. Ikuhara and M. W. Finnis, *Journal of the American Ceramic Society* **99**, 2016 (733).
45. T. Nakagawa, H. Nishimura, I. Sakaguchi, N. Shibata, K. Matsunaga, T. Yamamoto and Y. Ikuhara, *Scripta Materialia* **65**, 2011 (544).
46. I. Sakaguchi, V. Srikanth, T. Ikegami and H. Haneda, *Journal of the American Ceramic Society* **78**, 1995 (2557).
47. J. L. Meijering, in *Advances in Materials Research*, 5th ed, ed. H. Herman (Wiley-Interscience, New York, 1971).